

Development and characterization of Al₂O₃-based biocomposites reinforced with 3Y-TZP nanoparticles

C. M. F. A. Cossu¹, M. F. R. P. Alves¹, R. M. T. Gomes², K. Strecker³, R. O. Magnago^{1,2*}, C. Santos¹

¹Universidade do Estado do Rio de Janeiro, Faculdade de Tecnologia, 27537-000, Resende, RJ, Brazil

²Centro Universitário de Volta Redonda, 27240-560, Volta Redonda, RJ, Brazil

³Universidade Federal de São João Del Rei, 36307-352, São João Del Rei, MG, Brazil

Abstract

Alumina ceramics were reinforced with different amounts of stabilized-tetragonal zirconia nanoparticles, 3Y-TZP, and their properties were evaluated aiming for future applications in orthopedic medicine. Different amounts of 3Y-TZP (3 to 15 wt%) were mixed with Al₂O₃ powder, using high-energy milling (400 rpm-24 h). Samples were uniaxially compacted and sintered at 1600 °C-2 h. The samples were characterized by their relative density, microstructure, and crystalline phases. Furthermore, Vickers hardness, fracture toughness, and bending strength were determined. After the high-energy milling process, a considerable amount of monoclinic (m) ZrO₂ was detected in the powder mixtures, besides the α-Al₂O₃ and tetragonal (t) ZrO₂ phases. After sintering the samples presented relative densities greater than 98.5%, regardless of the amount of the Y-TZP additions used. Furthermore, the monoclinic phase was reconverted into the tetragonal phase during sintering. The Vickers hardness varied between 1750 and 1690 HV, depending on the amount of Y-TZP added. Bending strength and fracture toughness were also sensitive to the addition of Y-TZP, with values increasing from 351.5 to 701.7 MPa and K_{IC} from 3.5 to 5.6 MPa.m^{1/2}, indicating that the t-ZrO₂ grains enable the activation of the transformation toughening mechanisms such as t→m phase transformation and residual stress. The biological responses of the composites, evaluated by their cytotoxicity and chemical solubility, accredit the materials developed for future *in vitro* and *in vivo* studies aimed at application as biomaterials.

Keywords: bioceramics, Al₂O₃/Y-TZP composite, orthopedic medicine, mechanical properties.

INTRODUCTION

Alumina (Al₂O₃) is widely used as an important engineering material in many fields. However, its high brittleness represents a limiting factor for many applications [1-4]. Therefore, many scientists explore new methods to improve the fracture toughness and bending strength of Al₂O₃-based ceramics [5-10]. In particular, ceramic dental restorations exhibit high susceptibility to fracture under elevated compressive loads during mastication [11, 12]. Incorporating particle dispersions as structural reinforcement results in an increased toughness of the ceramic matrix. Specifically, the allotropic transformation of tetragonal (t) ZrO₂ into monoclinic (m) ZrO₂ absorbs energy which otherwise would result in crack propagation, as in the case of t-ZrO₂ particle dispersions in an Al₂O₃ matrix [13-15]. Nowadays a huge demand for ceramic materials for biomedical purposes exists and, in particular, yttrium-stabilized tetragonal zirconia polycrystals (3Y-TZP) are widely used for implants and reconstructions in dentistry [16]. Alumina-based composites with ZrO₂ additions as reinforcement exhibit increased fracture toughness and flexural strength when compared to pure Al₂O₃ ceramics. Several authors [17-20] investigated the influence of ZrO₂ additions of up to 5 vol% on the densification and mechanical

properties of Al₂O₃ ceramics.

Zirconia is often used as a reinforcing material in ceramic composites due to its excellent mechanical properties. Pure zirconia is monoclinic at room temperature and after heating up to 1170 °C it becomes tetragonal. With increasing temperature, its structure changes to a cubic fluorite that starts to appear at around 2370 °C. During cooling, the transformation from the tetragonal phase into the monoclinic phase is accompanied by a volumetric expansion of up to 4.5%, producing stresses close to the grain boundaries, leading to catastrophic failures in the densified material. To minimize these effects, some oxides such as CaO, MgO, Y₂O₃, or CeO₂ are added to ZrO₂ to stabilize the tetragonal phase, inducing a reduction in the stresses caused by the volumetric expansion and preventing the propagation of cracks in the material [21-23]. The tetragonal ZrO₂ particles embedded in the Al₂O₃ matrix undergo stress-induced phase transformation and micro-cracks form around existing alumina grains [24-26], resulting in an increase in the fracture toughness. Furthermore, an increasing grain size of the t-ZrO₂ phase increases the ability to trigger the transformation during fracture, and therefore the transformation toughness mechanism becomes predominant [27-31]. The phase transformation is martensitic in nature, following an athermal and diffusionless behavior with a thermal hysteresis plus a shear mechanism. The starting temperature of the martensitic transformation increases proportionally with increasing grain size of the tetragonal zirconia phase. This phenomenon is also directly related

*magnago@fat.uerj.br

 <https://orcid.org/0000-0002-9398-0639>

to the grain size distribution of zirconia in the composite. The fracture toughness of ZTA composites (alumina-based composites reinforced with ZrO_2) is controlled and optimized by the amount and grain size of the ZrO_2 particles. Reducing the grain size to a sub-micrometer level is advantageous over coarse-grained materials to improve strength and hardness. The mechanical properties of zirconia toughened alumina (ZTA) ceramics are closely related to different thermal properties, mainly the thermal expansion coefficient. Furthermore, thermal shock resistance is directly related to the maximum stress applied, the thermal conductivity, and the thermal expansion coefficient [32-35].

A noble and high-value-added application area for these ceramic biocomposites that is growing annually is orthopedic medicine, especially in applications such as components of femoral prostheses (ceramic joint balls). This importance increases due to the increase in life expectancy of the world population. Therefore, studies focused on presenting a set of properties necessary for use as a biomaterial associated with a usual processing technique are welcome. The objective of this work was to incorporate 3Y-TZP nanometric powder in an alumina matrix and evaluate the resulting mechanical properties and preliminary biological evaluation, aiming for future applications in orthopedic medicine.

EXPERIMENTAL

Commercial 3Y-TZP zirconia (TZ-3YSB-E, Tosoh, Japan) and alumina (CT-3000 SG, Almatiss) powders were used, which main characteristics are detailed in Table I. For the characterization of both powders, scanning electron microscopy (SEM) and X-ray diffraction (XRD) were used. The details of the procedures used for the characterization are described later.

Processing: at first, the nanocrystalline powders of ZrO_2 (3 mol% Y_2O_3), 3Y-TZP, and submicrometric Al_2O_3 were calcined at 700 °C for 120 min to remove residual organic binders. Then, a suspension with isopropyl alcohol was prepared adding Y-TZP in different proportions to Al_2O_3 . Mixtures composed of Al_2O_3 with additions of 3, 5, 10, and 15 wt% of 3Y-TZP were prepared using a mechanical stirrer for 120 min. Subsequently, the powders were subjected to high-energy grinding, using a mill (Pulverisett, Fritsch,

Germany), with Al_2O_3 balls and a grinding jar, for 24 h at 400 rpm. After milling, the powders were deagglomerated using a ball mill (MA-500, Marconi; 50 rpm) with two-shift alumina balls for 5 min and 1 min intervals between each shift, as well as movements in both directions. After deagglomeration, 5 wt% of PVA (polyvinyl alcohol) polymer as a binder was added. The powder mixtures containing binder were then homogenized by sieving through a 63 μm sieve. Cylindrical samples (n=15/group) with 15 mm diameter and 1.4 mm thickness were uniaxially compacted in two pressing stages: 1) pre-compaction at 50 MPa-30 s; and 2) 100 MPa-60 s. The compacts were sintered in an electric resistance heated furnace (F1650, Maitec). The sintering cycle adopted consisted of using a heating rate of 0.5 °C/min up to 600 °C, a 1 h hold, followed by further heating up to 1600 °C with a heating rate of 2 °C/min, and an isothermal holding time of 2 h. Cooling took place using a cooling rate of 5 °C/min until room temperature.

Characterizations: the compacted samples as well as the sintered samples were characterized by XRD analysis in a diffractometer (XRD-6000, Shimadzu). The analysis was conducted with $CuK\alpha$ radiation in the 2θ range of 20° to 80°, a step width of 0.05° and an exposure time of 5 s/step. The crystalline phases were identified using the Crystal Impact Match and the PDF-4-ICDD database (International Center for Diffraction Data, USA). The relative density of the sintered samples was determined as the ratio between the apparent density and the theoretical density (obtained by the rule of mixtures) of each mixture. The apparent density, in turn, was obtained using the Archimedes method. Sintered samples, representative of each prepared composition, were sanded and polished using an automatic polisher (Ecomet, Buehler, Germany). After polishing, the surfaces were cleansed in an ultrasonic bath and subjected to a thermal etching at 1500 °C for 15 min, with a heating rate of 15 °C/min, to reveal the grain boundaries. These surfaces were then metalized and observed by SEM (TM3030, Hitachi). The grain size distributions were determined using the Image J software, measuring around 500 grains per sample group.

Mechanical properties: the hardness and fracture toughness of the sintered samples were determined using the Vickers indentation method according to the ASTM C-1327-15 standard [36]. In this characterization, a microhardness

Table I - Characteristics of the raw materials used in this study (manufacturer's data).

Characteristic	Al_2O_3	3Y-TZP (ZrO_2 -3 mol% Y_2O_3)
	Almatiss: CT-3000 SG	Tosoh: ZPex
Purity	99.8%	99.7% (ZrO_2 + HfO_2 + Y_2O_3)
Average particle size (nm)	300	40
Specific surface area (m^2/g)	8.0	13.0
Density (g/cm^3)	3.98	6.05
Thermal expansion coefficient ($^{\circ}C^{-1}$)	8.5×10^{-6}	10.5×10^{-6}

tester (DHV-1000Z, Time) was used, applying an indentation load of 9.81 N. The fracture toughness obtained by the Vickers IF indentation technique, K_{IC} , was determined considering a c/a ratio <2.5 valid for the Palmqvist crack system, as proposed by Niihara [37], according to:

$$K_{IC} = 0.0084 \left(\frac{E}{HV} \right)^{0.4} \left(\frac{P}{a.l^{1/2}} \right) \quad (A)$$

where E is the theoretical Young's modulus (GPa), HV is the hardness (GPa), P is the applied load (N), a is the length of the indentation diagonal, and l is the crack length of indentation mark (mm). The flexural strength was determined by piston-on-3-ball (P-3B) testing, following the recommendations of the ISO 6872-15 standard [38]. The test was performed using $\phi 12 \times 1.3$ mm sintered disks in a universal testing machine (DL 10000, Emic, Brazil). During the test, a constant loading rate of 0.5 mm/min was used. The dimensions of the specimens were measured with a caliper. The flexural strength, σ_f (MPa), was calculated by:

$$\sigma_f = \frac{-0.2387.N.(X-Y)}{b^2} \quad (B)$$

$$X = (1+\nu) \ln \left(\frac{r_2}{r_3} \right)^2 + \frac{1-\nu}{2} \left(\frac{r_2}{r_3} \right)^2 \quad (C)$$

$$Y = (1+\nu) \left[1 + \ln \left(\frac{r_2}{r_3} \right)^2 \right] + (1-\nu) \left(\frac{r_1}{r_3} \right)^2 \quad (D)$$

where N is the maximum force (N), ν is the Poisson's ratio (0.25), r_1 is the radius of the supporting circle (5.50 mm), r_2 is the radius of the loading area (0.70 mm), r_3 is the specimen radius (mm), and b is the specimen thickness (mm). The statistical analysis of flexural strength was carried out using Weibull statistics [39]. The two-parameter Weibull distribution function was determined according to:

$$P = 1 - \exp \left[\left(- \frac{\sigma}{\sigma_0} \right)^m \right] \quad (E)$$

where P is the failure probability, m is the Weibull modulus, σ_0 is the characteristic stress (MPa), and σ is the fracture stress (MPa). The Weibull parameters m and σ_0 were obtained by transforming Eq. E into:

$$\ln \ln \left(\frac{1}{1-P} \right) = m \cdot \ln \sigma - m \ln \sigma_0 \quad (F)$$

and plotting $\ln \ln [1/(1-P)]$ versus $\ln \sigma$. The characteristic stress, σ_0 , corresponding to 63.2% failure probability, was estimated as a reference and compared to the average stress values.

Cytotoxicity and chemical solubility: the *in vitro* cytotoxicity test was performed according to ISO 10993-5 [40], by the neutral red uptake methodology (negative control: high-density polyethylene; positive control: natural rubber latex film). Further details of this experiment were reported by Santos et al. [41]. A chemical solubility test

was performed in duplicate, using an acetic acid solution (4 vol%) in distilled water. Clean and dry samples were weighed with an analytical balance (precision 0.1 mg) and then immersed in 100 mL of the acetic acid solution at 80 °C for 16 h. Then the samples were washed in distilled water, dried at 150 °C-4 h, and reweighed. The mass difference between samples before and after the chemical solubility test indicated the chemical solubility of the material.

RESULTS AND DISCUSSION

Characterization of powders and sintered samples

Fig. 1 presents SEM images of the starting powders used, showing spherical agglomerates formed by spray-drying. Fig. 2 presents the results of the X-ray diffraction analysis of the compacted and sintered samples, respectively. The XRD results of the compacted samples (Fig. 2a) indicated the presence of Al_2O_3 , $m-ZrO_2$, and $t-ZrO_2$ as crystalline phases. The presence of monoclinic ZrO_2 was due to the milling process used in the homogenization of the mixtures, due to mechanical impacts between the particles. After the sintering process at 1600 °C-2 h (Fig. 2b), the diffractograms revealed that the sintering process was effective, promoting the reconstruction of the tetragonal phase $m \rightarrow t-ZrO_2$. However, samples containing 15 wt% of ZrO_2 still showed some low-intensity $m-ZrO_2$ peaks, suggesting that although the Al_2O_3 matrix restricts the $t \rightarrow m-ZrO_2$ transformation during cooling, the samples presented residual stresses during cooling that favored the allotropic transformation.

The SEM micrographs presented in Fig. 3 show the microstructure of the sintered samples with different ZrO_2 additions. Zirconia grains (light phase) with a grain size smaller than 1 μm were homogeneously distributed in the Al_2O_3 matrix (gray phase). It was observed that the ZrO_2 grains were located at the grain boundaries of the Al_2O_3 matrix. The location of the ZrO_2 grains at the grain boundaries of the Al_2O_3 matrix influenced the grain growth of the Al_2O_3 grains, resulting in a decrease of the average Al_2O_3 grain size with increasing amount of ZrO_2 particles added. The inhibition of the grain growth of ceramic matrix grains due to a secondary dispersed phase has also been observed in previous works [42-44]. Fig. 4 presents a summary of the grain sizes of Al_2O_3 and ZrO_2 , as well as of the fracture toughness of the sintered composites as a function of the Y-TZP content. After applying a load of 9.81 N, the cracks formed were of the Palmqvist type with a c/a ratio varying between 0.65 and 1.06. As shown in Fig. 4, an increasing amount of ZrO_2 particles in composition led to a decrease in the average grain size of Al_2O_3 , diminishing from 4.5 μm (3 wt% ZrO_2) to 2.5 μm (15 wt% ZrO_2). According to previous works, cracks in ZTA ceramic materials tend to propagate along grain boundaries (intergranular fracture). Part of this fracture energy stimulates the allotropic transformation mechanism $t-ZrO_2 \rightarrow m-ZrO_2$ at the grain boundaries, thus impeding crack propagation [45, 46]. This mechanism is the reason for the observed increase in fracture toughness

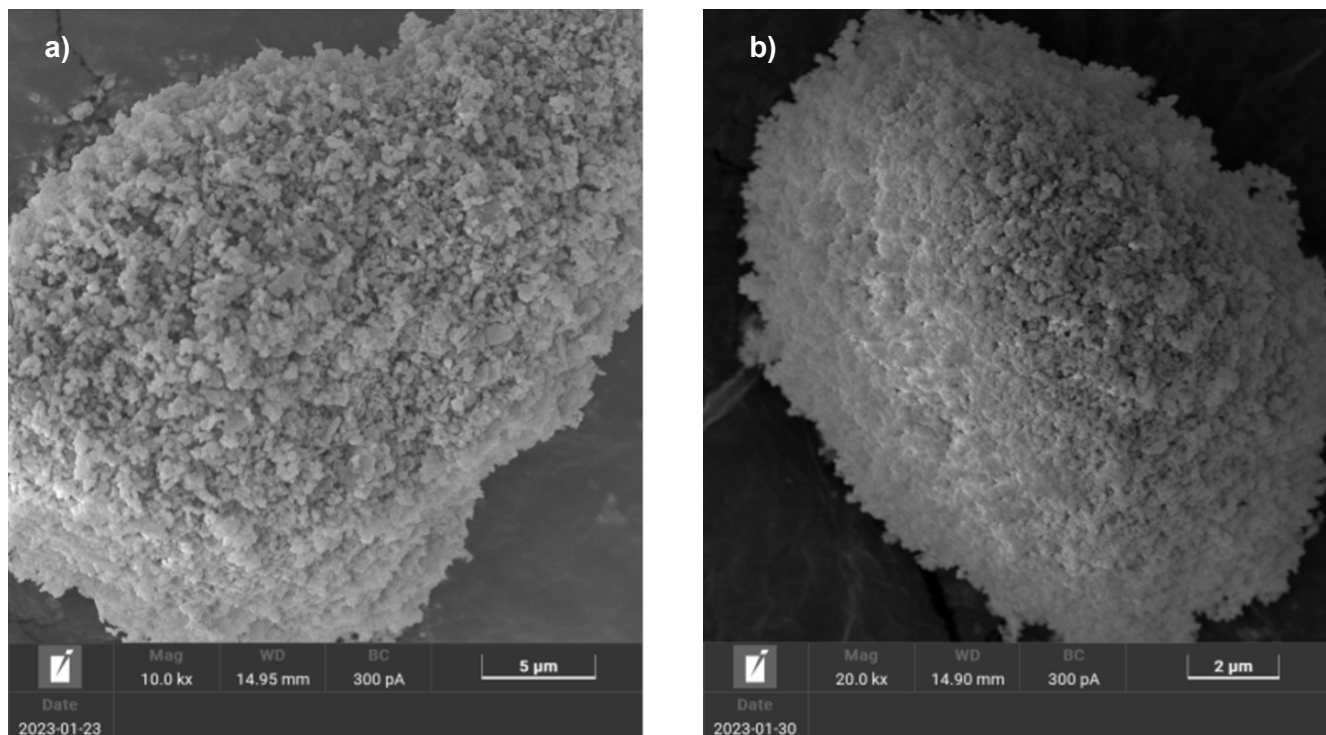


Figure 1: SEM micrographs of the starting (agglomerated) powders: a) Al_2O_3 ; and b) 3Y-TZP.

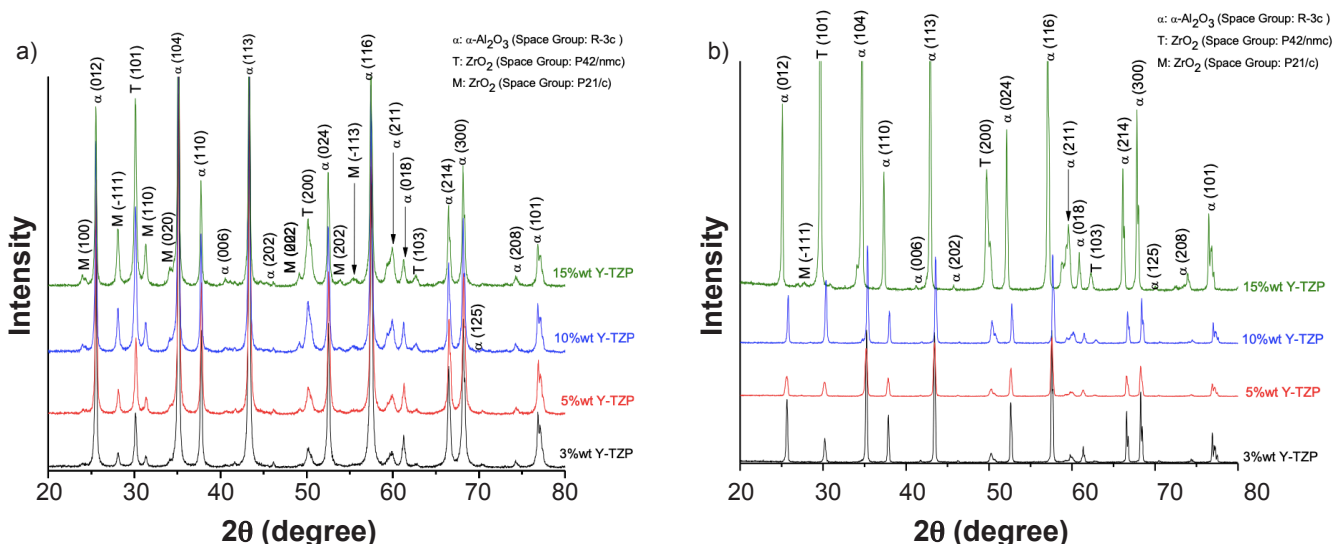


Figure 2: XRD patterns of: a) compacted powder mixtures; and b) sintered (1600 °C-2 h) composites.

from 3.54 to 5.62 $\text{MPa}\cdot\text{m}^{1/2}$ in the composite materials when increasing the ZrO_2 concentration from 3 to 15 wt% ZrO_2 .

Fig. 5 shows the influence of increasing ZrO_2 concentration on the densification and hardness of the Al_2O_3 - ZrO_2 composites. Increasing amounts of ZrO_2 improved the sinterability of the Al_2O_3 matrix, promoting higher densification of samples sintered at 1600 °C-2 h. On the other hand, hardness decreased linearly as a function of increasing ZrO_2 concentration, diminishing from 1750 HV (3 wt% ZrO_2) to 1690 HV (15 wt% ZrO_2). The decrease in hardness in the materials produced was associated with

the hardness difference between the two components, where the hardness of ZrO_2 (1300 HV [47]) is lower than the hardness of Al_2O_3 (1900 HV [48]). Fig. 6 shows the influence of ZrO_2 concentration on the Weibull statistics of composites sintered at 1600 °C-2 h. Although the standard suggests that the test to determine the Weibull modulus be carried out on 30 specimens, the Weibull modulus (m) was $m=7.3$ (3 wt% ZrO_2), $m=4.7$ (5 wt% ZrO_2), $m=12.8$ (10 wt% ZrO_2), and $m=8.1$ (15 wt% ZrO_2) for 10 specimens tested in each condition. This significant increase of around 270% represents a significant increase in the reliability of the

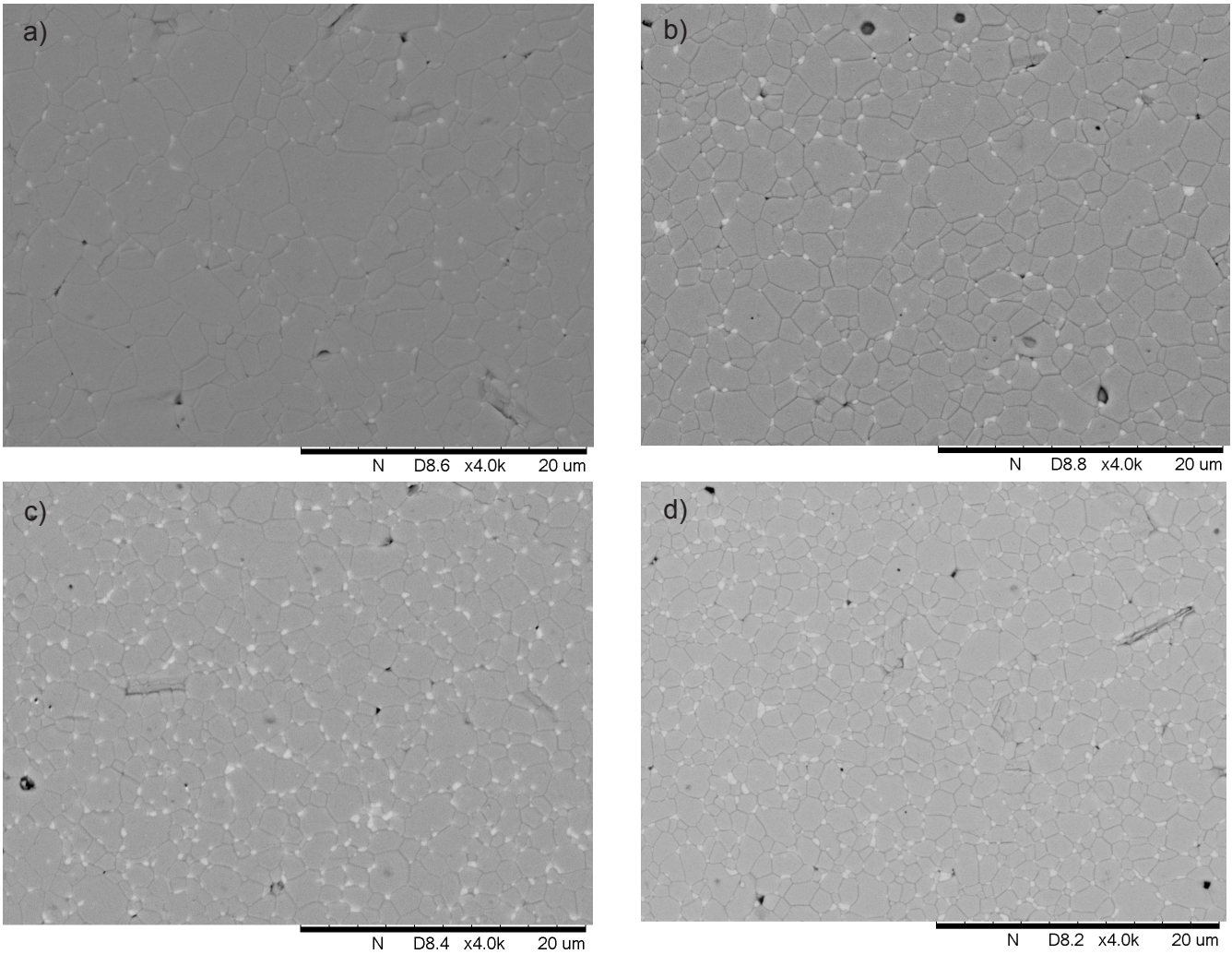


Figure 3: SEM micrographs of the Al_2O_3 composites containing different amounts of 3Y-TZP: a) 3 wt%; b) 5wt%; c) 10 wt%; and d) 15 wt%.

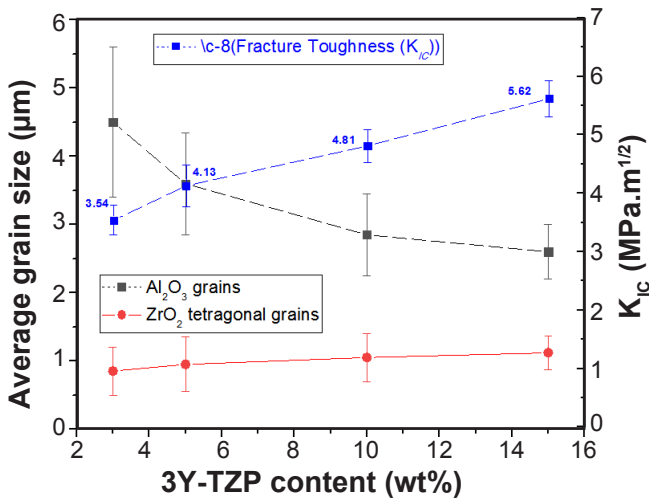


Figure 4: Average grain size of ZrO_2 and Al_2O_3 grains and fracture toughness (K_{Ic}) of the composites after sintering at 1600 °C-2 h.

composites produced. The brittle fracture of ceramics such as alumina is associated with residual porosity, microstructure

(grain size), and grain morphology, with crack deflection as the main toughening mechanism, in the case of ceramics that present intergranular fracture [49]. The gains in reliability, denoted by the increase of the Weibull modulus, infer that the Y-TZP grains, known to possess toughening mechanisms by phase transformation, are fundamental for the refinement of the microstructure of the alumina matrix, in addition to improving the densification of composites.

A proposed mathematical model allows for determining the mechanical strength from E , ν , and a [50]. The variables presented in Table II were determined using the rule of mixture for ceramic materials. Table II shows the results of fracture energy (γ), flaw size (a), and mechanical strength (σ_f) of the samples after sintering at 1600 °C-2 h, obtained by the relation proposed by Irwin. The corroboration of the results with other authors showed the toughening effect of ZrO_2 on the Al_2O_3 matrix. The influence of the ZrO_2 concentration was determinant in increasing the mechanical strength of the samples from 351 to 701 MPa for samples containing 3 to 15 wt% ZrO_2 , respectively. According to the linear elastic fracture mechanics, the mechanical strength of

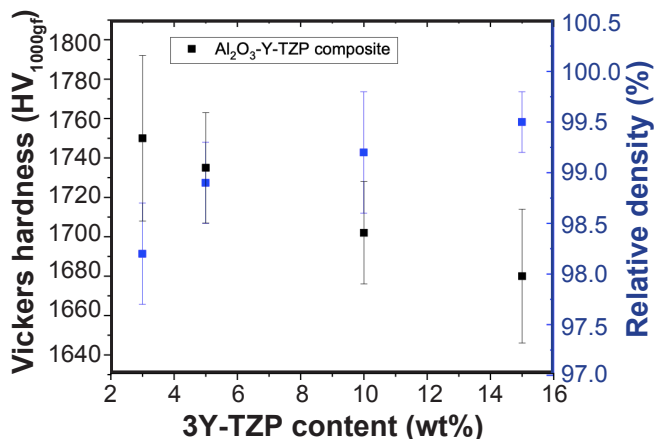


Figure 5: Vickers hardness and relative density of the $\text{Al}_2\text{O}_3\text{-ZrO}_2$ composites sintered at $1600\text{ }^\circ\text{C-2 h}$.

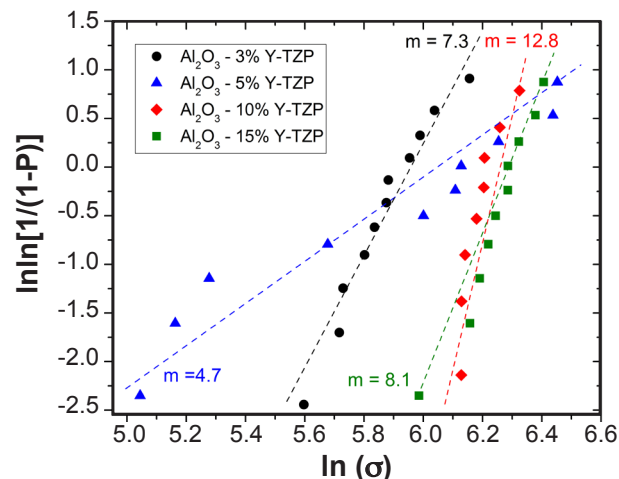


Figure 6: Weibull plots of the fracture strength distributions of composites containing 3, 5, 10, and 15 wt% of Y-TZP sintered at $1600\text{ }^\circ\text{C-2 h}$.

Table II - Mechanical parameters used in the strength analysis.

Material	Young's modulus, E (GPa)	Poisson's ratio, ν	K_{IC} ($\text{MPa}\cdot\text{m}^{1/2}$)	γ_i (J/m^2)	a (μm)	σ_f (MPa)
Al_2O_3	380.0	0.220	-	-	-	-
Y-TZP ($\text{ZrO}_2\text{-3 mol\% Y}_2\text{O}_3$)	195.0	0.250	-	-	-	-
$\text{Al}_2\text{O}_3/\text{Y-TZP (97-3)}$	374.4	0.221	3.54	10.3	25.7	351.5
$\text{Al}_2\text{O}_3/\text{Y-TZP (95-5)}$	370.7	0.221	4.13	10.6	11.5	613.5
$\text{Al}_2\text{O}_3/\text{Y-TZP (90-10)}$	361.5	0.223	4.81	10.3	14.1	645.2
$\text{Al}_2\text{O}_3/\text{Y-TZP (85-15)}$	352.2	0.225	5.62	14.5	16.3	701.7

a material is defined by the Irwin equation:

$$\sigma_f = \frac{K_{IC}}{Y \cdot a^{1/2}} \quad (\text{G})$$

where K_{IC} is the fracture toughness, a is the natural flaw size, and Y is the dimensionless calibration factor ($Y=1.4$ [51]). The fracture toughness can also be associated with the fracture energy (γ_i) by:

$$K_{IC} = \sqrt{2 \cdot E \cdot \gamma_i} \quad (\text{H})$$

where E is the Young's modulus. These equations determine that the mechanical strength of a ceramic material can be characterized by three factors: the flaw size, Young's modulus, and the fracture energy. Based on classical equations from the fracture mechanics of brittle materials it is possible to predict the fracture energy and calculate the critical flaw size. Table II also presents calculated values of the theoretical fracture energy and the critical flaw size, using the experimental results obtained, which were close to consistent values. Critical flaw sizes of 11 to $25\ \mu\text{m}$ may be present in regions of maximum stress such as the

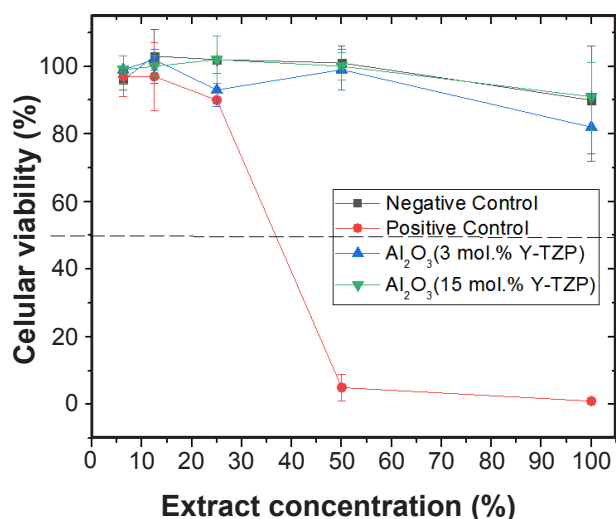
tensile surface and during bending would be the main factor responsible for the failure of the materials. However, one must consider the effect of the reduction of residual porosity, identified by the increase in densification in composites with higher Y-TZP contents, in addition to the higher amount of zirconia particles, which were well dispersed in the Al_2O_3 matrix and that acted as regions of shielding for the crack growth. The ZrO_2 grains induced the toughening mechanisms by the $t \rightarrow m$ transformation and microcracking, in addition to compressive residual thermal stresses, resulting in increased fracture toughness and flexural strength of the composites.

Preliminary biological assessment

Fig. 7 shows the cytotoxicity results of the sintered samples for composites containing 3% and 15% Y-TZP. The results indicated that the composites exhibited a non-cytotoxic behavior and therefore are biocompatible since all samples showed similar behavior to the negative control. Only the positive control showed 34% cytotoxicity, i.e. an extract concentration of 34% caused death in 50% of the cell population. The cytotoxicity index ($\text{IC}_{50\%}$) is found as the point of intersection between the curve of cell viability

Table III - Results of the chemical solubility testing.

Material	Initial mass (mg)	Mass after acetic acid solution 4% v/v (mg)	Mass, final measurement after drying at 150 °C-4 h (mg)
ZrO ₂ (3% Y ₂ O ₃)	2.3	2.3	2.3
Al ₂ O ₃ /Y-TZP (97-3)	1.1	1.09	1.09
Al ₂ O ₃ /Y-TZP (85-15)	1.0	0.99	0.98

Figure 7: Results of cytotoxicity test on Al₂O₃ samples sintered with 3% and 15% Y-TZP.

and the line of 50% viability, as shown in Fig. 7. Table III shows the results of the chemical solubility test of the sintered composites containing 3% and 15% Y-TZP, and 100% Y-TZP as reference. Based on the weight loss between the samples before and after the chemical solubility tests which is an important property for application in biological systems such as prostheses or implants, it can be stated that the composites presented high chemical stability. This information, even if only on a preliminary basis, classifies the composites for future biological applications.

CONCLUSIONS

The beneficial effects of the reinforcement of alumina ceramics with t-ZrO₂ nanoparticles on the microstructural development and the mechanical properties were demonstrated. The ZrO₂ grains located at the grain boundaries of the Al₂O₃ matrix significantly reduced the grain growth of the Al₂O₃ grains with increasing amounts of ZrO₂ particles added. The grain size of the Al₂O₃ grains was reduced from 4.5 to 2.5 μm when 3 to 15 wt% ZrO₂ particles were added, representing a decrease of about 55%. The transformation toughening mechanism of t-ZrO₂ into m-ZrO₂, besides the smaller average grain size, resulted in a significant increase in bending strength (351 to 701 MPa) and fracture toughness from 3.54 to 5.62 MPa.m^{1/2} when increasing the ZrO₂ concentration from 3 to 15 wt% ZrO₂.

At the same time, an increased reliability of the composites, as expressed by a higher Weibull modulus (m), was also observed, which increased from m=4.7 to m=12.8. On the other hand, a decrease of hardness with increasing amount of ZrO₂ was noted, diminishing from 1750 HV (3 wt% ZrO₂) to 1690 HV (15 wt% ZrO₂). Finally, the preliminary biological evaluation by cytotoxicity and chemical solubility tests demonstrated the potential of the Al₂O₃/3Y-TZP biocomposite for future orthopedic applications, presenting satisfactory biological and chemical stability, combined with the high mechanical properties mentioned above; however, tribological evaluations under hydrothermal degradation conditions must be carried out to make these bioceramics suitable for *in vivo* testing.

ACKNOWLEDGMENTS

The authors would like to thank FAPERJ (Carlos Chagas Research Support Foundation of the State of Rio de Janeiro) and CNPq (National Council for Scientific and Technological Development) for financial support of this project.

REFERENCES

- [1] D.T. Jiang, K. Thomson, J.D. Kuntz, J.W. Ager, A.K. Mukherjee, *Scr. Mater.* **56** (2007) 959.
- [2] J. Lalande, S. Scheppokat, R. Janssen, *J. Eur. Ceram. Soc.* **22** (2002) 2165.
- [3] D. Casellas, M.M. Nagl, L. Llanes, *J. Mater. Process. Technol.* **143** (2003) 148.
- [4] D. Wenya, A. Yunlong, H. Wen, C. Weihua, L. Bing, L. Chen, *Ceram. Int.* **46**, 6 (2020) 8452.
- [5] K. Novoselov, A. Geim, S. Morozov, *Science* **306** (2004) 666.
- [6] Y.F. Chen, J.Q. Bi, C.L. Yin, *Ceram. Int.* **40** (2014) 13883.
- [7] Y. Liu, C. Ramirez, L. Zhang, W.W. Wu, N.P. Padture, *Acta Mater.* **127** (2017) 203.
- [8] W. He, Y.L. Ai, B.L. Liang, W.H. Chen, C.H. Liu, *Mater. Sci. Eng. A* **723** (2018) 134.
- [9] Y. Liu, Y.L. Ai, W. He, W.H. Chen, J.J. Zhang, *Ceram. Int.* **44** (2018) 16421.
- [10] F. Sommer, R. Landfried, F. Kern, R. Gadow, *J. Eur. Ceram. Soc.* **32** (2012) 4177.
- [11] A. Nevarez-Rascon, A. Aguilar-Elguezabal, E. Orrantia, M.H. Bocanegra-Bernal, *Int. J. Refract. Met. Hard Mater.* **27**, 6 (2009) 962.

- [12] T. Linkevicius, E. Vladimirovas, S. Grybauskas, A. Puisys, V. Rutkunas, *Stomatologija* **10** (2008) 133.
- [13] N. Saheb, K. Mohammad, *Ceram. Int.* **42** (2016) 12330.
- [14] J.L. Liu, Y.G. Wang, F.Q. Yang, K.P. Chen, L.N. An, *J. Alloys Compd.* **622** (2015) 596.
- [15] D. Sarkar, S. Adak, M.C. Chu, S.J. Cho, N.K. Mitra, *Ceram. Int.* **33**, 2 (2007) 255.
- [16] E.B.B. Jalkh, K.N. Monteiro, P.F. Cesar, L.A. Genova, E.T.P. Bergamo, A.C.O. Lopes, E. Lima, P.N. Lisboa-Filho, T.M.B. Campos, L. Witek, P.G. Coelho, A.F.S. Borges, E.A. Bonfante, *Dent. Mater.* **36**, 9 (2020) 1190.
- [17] M. Ipek, S. Zeytin, C. Bindal, *J. Alloys Compd.* **509** (2011) 486.
- [18] M. Khoshkalam, M.A. Faghihi-Sani, A. Nojoomi, *Trans. Indian Ceram. Soc.* **72** (2013) 175.
- [19] C. Meunier, F. Zuo, N. Peillon, S. Saunier, S. Marinell, D. Goeuriot, *J. Am. Ceram. Soc.* **100** (2016) 1.
- [20] M.C. Aragón-Duarte, A. Nevarez-Rascón, H.E. Esparza-Ponce, M.M. Nevarez-Rascón, R.P. Talamantes, C. Ornelas, J. Mendez-Nonell, J. González-Hernández, M.J. Yacamán, A. Hurtado-Macías, *Ceram. Int.* **43** (2017) 3931.
- [21] J.R. Kelly, I. Denry, *Dent. Mater.* **24** (2008) 289.
- [22] I. Denry, J.R. Kelly, *Dent. Mater.* **24** (2008) 299.
- [23] J.K.M.F. Daguano, C. Santos, R.C. Souza, R.M. Balestra, K. Strecker, C.N. Elias, *Int. J. Refract. Met. Hard Mater.* **25** (2007) 374.
- [24] K. Tsukuma, K. Ueda, M. Shimda, *J. Am. Ceram. Soc.* **68**, 1 (1985) C4.
- [25] V.V. Srdic, L. Radonjic, *J. Am. Ceram. Soc.* **80**, 8 (1997) 2056.
- [26] A.H. Heuer, N. Clausen, W.M. Kriven, M. Rühle, *J. Am. Ceram. Soc.* **65**, 12 (1982) 642.
- [27] D.J. Green, *J. Am. Ceram. Soc.* **65**, 12 (1982) 610.
- [28] G.M. Wolten, *J. Am. Ceram. Soc.* **46** (1963) 418.
- [29] J. Wang, M. Rainforth, R. Stevens, *Br. Ceram. Trans. J.* **88** (1989) 1.
- [30] M.V. Swain, *J. Mater. Sci. Lett.* **5** (1986) 1159.
- [31] P.F. Becher, M.V. Swain, *J. Am. Ceram. Soc.* **20** (1992) 1178.
- [32] H. Gletter, *Prog. Mater. Sci.* **33** (1989) 223.
- [33] G.W. Nieman, J.R. Weertman, R.W. Siegel, *J. Mater. Res.* **6** (1991) 1012.
- [34] D. Sarkar, S. Adak, N.K. Mitra, *Compos. A Appl. Sci. Manuf.* **38**, 1 (2007) 124.
- [35] G.R. Anstis, P. Chantikul, B.R. Lawn, D.B. Marshall, *J. Am. Cer. Soc.* **64** (1981) 533.
- [36] ASTM C1327-15, “Standard test method for Vickers indentation hardness of advanced ceramics” (1999).
- [37] K. Niihara, *J. Mater. Sci. Lett.* **2** (1983) 221.
- [38] ISO 6872, “Dentistry: dental ceramics”, *Int. Org. Stand.* (2015).
- [39] R. Danzer, P. Supancic, J. Pascual, T. Lube, *Eng. Fract. Mech.* **74**, 18 (2007) 2919.
- [40] ISO 10993-5, “Biological evaluation of medical devices, part 5: tests for cytotoxicity: in vitro methods” (1992).
- [41] C. Santos, S. Ribeiro, J.K.M.F. Daguano, S.O. Rogero, K. Strecker, C.R.M. Silva, *Sci. Eng.* **27** (2007) 148.
- [42] G.J. Liu, H.B. Qiu, R. Todd, R.J. Brook, J.K. Guo, *Mater. Res. Bull.* **33**, 2 (1998) 281.
- [43] M.M. Coutinho, A.C.P. Nascimento, J.E.V. Amarante, C. Santos, J.L.A. Ferreira, C.R.M. Silva, *Mater. Res.* **25** (2022) e20220199.
- [44] C. Santos, L.H.P. Teixeira, J.K.M.F. Daguano, K. Strecker, C.N. Elias, *Mater. Sci. Forum* **530-531** (2006) 526.
- [45] S. Deville, J. Chevalier, G. Fantozzi, J.F. Bartolomé, J. Requena, J.S. Moya, R. Torrecillas, L.A. Díaz, *J. Eur. Ceram. Soc.* **23** (2003) 2975.
- [46] D. Casellas, M.M. Nagl, L. Llanes, M. Anglada, *J. Am. Ceram. Soc.* **88** (2005) 1958.
- [47] C. Santos, L.H.P. Teixeira, J.K.M.F. Daguano, S.O. Rogero, K. Strecker, C.N. Elias, *Ceram. Int.* **35** (2009) 709.
- [48] S. Yang, S. Yang, Y. Zhu, L. Fan, M. Zhang, *J. Eur. Ceram. Soc.* **42** (2022) 202.
- [49] R.C. Bradt, D.P.H. Hasselman, D. Munz, M. Sakai, V. Ya Shevchenko, “Fracture mechanics of ceramics” **10**, Springer Sci., New York (2013) 655.
- [50] S. Bueno, C. Baudin, *Bol. Soc. Esp. Ceram. V.* **46** (2007) 103.
- [51] R.L. Carlson, G.A. Kardomateas, J.I. Craig, in “Mechanics of failure mechanisms in structures”, Springer, Dordrecht (2012) 187.

(Rec. 10/07/2023, Rev. 07/10/2023, Ac. 25/10/2023)

